Journal of Applied Electrochemistry (2006) 36:355–362
DOI 10.1007/s10800-005-9072-0

Carbon supported Pt–Cr alloys as oxygen-reduction catalysts for direct methanol fuel cells

E. ANTOLINI[1], J.R.C. SALGADO[1], L.G.R.A. SANTOS[1], G. GARCIA[1], E.A. TICIANELLI[1], E. PASTOR[2] and E.R. GONZALEZ[1,*]
[1]*Instituto de Química de São Carlos, USP, C.P. 780 São Carlos, SP 13560-970, Brazil*
[2]*Departamento de Química Física, Universidad de La Laguna, 38071, La Laguna, España*
*(*author for correspondence +55-0-16-3373-9952, e-mail: ernesto@iqsc.usp.br)*

Received 27 July 2005; accepted in revised form 13 September 2005

Key words: electrocatalysis, methanol tolerance, oxygen reduction, PEM fuel cell, Pt–Cr alloy

Abstract

Electrocatalytic activities of various carbon-supported platinum–chromium alloy electrocatalysts towards oxygen reduction in 1 mol l^{-1} H_2SO_4 and in 1 mol l^{-1} H_2SO_4/1–3 mol l^{-1} CH_3OH, were investigated by means of rotating disc electrode experiments and in solid polymer electrolyte direct methanol fuel cells. The activity of these electrocatalysts for methanol oxidation was evaluated using cyclic voltammetry. It was found that Pt_9Cr/C prepared by reduction with $NaBH_4$ exhibits the lowest activity for methanol oxidation and the highest activity for oxygen reduction in the presence of methanol, in comparison to commercial Pt/C, Pt_3Cr/C and PtCr/C electrocatalysts.

1. Introduction

Direct methanol fuel cells (DMFCs) are promising electrochemical energy converters for a variety of applications because of the system simplicity. The liquid-feed system does not require any fuel processing equipment and can be operated even at room temperatures. Another advantage of the DMFC is the fact that it does not require complex humidification and heat management modules, as in the hydrogen fed proton exchange membrane (PEM) fuel cell system, because the dilute methanol water mixtures entering the DMFC provide the necessary humidification and heat control. These advantages allow the DMFC to be customized for use in portable electronic devices [1].

The crossover of methanol from the anode to the Pt-based oxygen cathode is one of the major practical problems limiting the performance of the direct methanol fuel cell [2–6]. The mixed potential, which results from the oxygen reduction reaction and the methanol oxidation occurring simultaneously, reduces the cell voltage, generates additional water and increases the required oxygen stoichiometric ratio.

To overcome this problem, a common action is to test the activity for the oxygen reduction reaction (ORR) in the presence of methanol of some platinum alloys with first-row transition metals which present a higher activity for the ORR than pure platinum in low temperature fuel cells operated on hydrogen, and use them as DMFC cathode electrocatalysts [7–12]. The improvement in the ORR electrocatalysis has been ascribed to different factors such as changes in the Pt–Pt interatomic distance [13], the surface area [14] and, particularly, the Pt electronic configuration [15]. Toda et al. [15] proposed a new mechanism for the enhancement of the ORR on Pt–M alloys, based on an increase of d-electron vacancies of the thin Pt surface layer caused by the underlying alloy. On the basis of their model, such an increase of 5d vacancies leads to an increased 2π electron donation from the oxygen to the surface Pt atoms, resulting in an increased O_2 adsorption and a weakening of the O–O bond, enhancing in this way the kinetics of the ORR. In a work with X-ray absorption spectroscopy (XAS), Mukerjee et al. [16] explained the enhanced electrocatalysis of Pt-based alloys on the basis of the interplay between the electronic (Pt d-vacancy) and geometric factors (Pt coordination number) and their effect on the chemisorption behaviour of OH species from the electrolyte.

The ensemble effects where the dilution of the active component with the catalytically inert metal changes the distribution of active sites, open different reaction pathways [17], and can explain the enhanced methanol-resistance of the Pt-based alloys. The dissociative chemisorption of methanol requires the existence of several adjacent Pt ensembles [18, 19]. Thus the presence of atoms of the second metal around Pt active sites could block methanol adsorption on Pt sites due to a dilution effect. Consequently, methanol oxidation on the binary-component electrocatalyst is reduced. On the

other hand, oxygen adsorption, which usually can be regarded as dissociative chemisorption, requires only two adjacent sites.

The oxygen-reduction kinetics on carbon-supported nanosized Pt–Cr alloy catalysts was studied by Yang et al. [7] using the rotating disk electrode technique in pure and methanol-containing electrolytes. The Vulcan XC-72 carbon-supported Pt–Cr alloy catalysts with different Pt/Cr atomic ratios were prepared via a Pt-carbonyl route. The bimetallic Pt–Cr alloy catalysts with the different Pt/Cr atomic ratios exhibited much higher methanol tolerance during the ORR than the Pt/C catalyst. Furthermore, the catalytic activity for methanol oxidation on the Pt–Cr alloy electrocatalysts was much lower than that on the Pt/C electrocatalyst.

In this work, carbon supported Pt–Cr electrocatalysts were prepared by reduction with $NaBH_4$ and the electrochemical properties were compared with commercial Pt/C, Pt_3Cr/C and PtCr/C. Studies were made using the thin film rotating disk electrode technique in pure and methanol-containing electrolytes, and also in a direct methanol fuel cell (DMFC).

2. Experimental

Commercially available Pt-based fuel cell electrocatalysts provided by E-TEK (Natick, MA), were 20 wt. % Pt supported on Vulcan XC-72 carbon black (Cabot), Pt_3Cr and PtCr alloy electrocatalyst, also 20 wt. % metal on Vulcan XC-72.

2.1. *Preparation of the carbon supported Pt–Cr electrocatalyst*

The carbon supported Pt–Cr electrocatalyst was prepared by reduction of the ionic precursors (in the atomic ratio 75:25) with sodium borohydride [20, 21]. The electrocatalyst was prepared by impregnating high surface area carbon (Vulcan XC-72) with a chloroplatinic acid solution and a chromium chloride ($CrCl_3 \cdot 6H_2O$) solution. The metals were then reduced with a sodium borohydride solution, which was slowly added under sonication. This procedure will be called the borohydride method (BM). The electrocatalyst was 20 wt. % metal on carbon.

2.2. *Physical characterization of Pt/C and Pt–Cr/C electrocatalysts*

The atomic ratios of the Pt–Cr/C electrocatalysts were determined by energy dispersive X-ray analysis (EDX) coupled to a scanning electron microscopy LEO Mod. 440 with a silicon detector with Be window and applying 20 keV.

X-ray diffractograms of the electrocatalysts were obtained in a universal diffractometer Carl Zeiss-Jena, URD-6, operating with Cuk_α radiation ($\lambda = 0.15406$ nm) generated at 40 kV and 20 mA. Scans were done at $3° \text{ min}^{-1}$ for 2θ values between 20 and 100°. In order to estimate the particle size from XRD Scherrer's equation was used [22]. For this purpose, the (220) peak of the Pt fcc structure around $2\theta = 70°$ was selected. In order to improve the fitting of the peak, recordings for 2θ values from 60 to 80° were done at $0.02° \text{ min}^{-1}$. The lattice parameters were obtained by refining the unit cell dimensions by the least squares method [23].

2.3. *Electrode preparation and electrochemical characterization of Pt/C and Pt–Cr/C electrocatalysts*

A conventional one-compartment glass cell with a Luggin capillary was used in the electrochemical experiments employing liquid electrolyte. A large area platinized platinium foil served as the counter electrode and a reversible hydrogen electrode (RHE) system was used as the reference electrode. These experiments were carried out in 0.5 mol l^{-1} H_2SO_4, prepared from high purity reagents (Merk) and water purified in a Milli-Q (Millipore) system. The electrolyte was satured with pure N_2 or O_2 gases (White Martins), depending on the experiments.

Experiments were carried out in the range of potentials from 1.1 to 0.1 V using an AUTOLAB potentiostat (PGSTAT30). Steady state polarization curves were recorded at several rotation rates to evaluate the ORR kinetic parameters. All the experiments were conducted at room temperature (25 ± 1 °C).

The working electrodes were composed of the metal/C catalysts deposited as a thin layer over a pyrolitic graphite disk of a rotating ring/disk electrode (RRDE). A pyrolitic carbon disk, 5 mm diameter (0.196 cm^2) was used as substrate for the metal/C catalyst. An aqueous suspension of 1.0 mg ml^{-1} of the metal/C was prepared by ultrasonically dispersing it in pure water (Millipore). An aliquot of the dispersed suspension was pipetted on the top of the pyrolitic carbon substrate surface and dried at ambient temperature. After preparation, the electrode was immersed into the deareted 0.5 mol l^{-1} H_2SO_4 electrolyte. In the RRDE system, the ring electrode (platinum) was used to sensor the H_2O_2 produced in the working disk electrode. This was made by measuring the magnitude of the H_2O_2 oxidation current at a constant potential of 1.2 V vs. RHE, where the oxygen reduction current is negligible.

The ORR was also studied in the presence of 1–3 mol l^{-1} methanol solutions in H_2SO_4. Before each experiment, the electrode support was polished with a Al_2O_3 suspension in water, particle size 0.05 μm, and cleaned ultrasonically in high purity water for 2 min.

In order to test the electrochemical behaviour in a single DMFC fed with methanol/oxygen, the electrocatalysts were used to make two layer gas diffusion electrodes (GDE). A diffusion layer was made with carbon powder (Vulcan XC-72) and 15 wt. % polytetrafluoroethylene (PTFE) and applied over a carbon cloth (PWB-3, Stackpole). On top of this layer, the electrocatalyst was applied in the form of a homogeneous dispersion of Pt–Cr/C, or Pt/C, Nafion® solution

(5 wt. %, Aldrich) and isopropanol (Merck). All the GDEs were made to contain 1 mg Pt cm^{-2}.

For the direct methanol single cells studies, the electrodes were hot pressed on both sides of a Nafion® 117 membrane at 125 °C and 50 kg cm^{-2} for 2 min. Before using them, the Nafion® membranes were treated with a 3 wt. % solution of H_2O_2, washed and then treated with a 0.5 mol l^{-1} solution of H_2SO_4. The geometric area of the electrodes was 4.62 cm^2, and the anode material was 20 wt. % Pt/C E-TEK. The cell polarization data at 90 °C were obtained by circulating a 2 mol l^{-1} aqueous methanol solution at the anode and oxygen at 3 atm pressure at the cathode.

3. Results and discussion

The composition of the Pt–Cr/C electrocatalysts was determined by EDX analysis. As shown in Table 1, it was found that the EDX composition of the commercial Pt_3Cr/C and PtCr/C electrocatalysts was close to the nominal value. On the other hand, the Cr content of the electrocatalyst prepared by the BM was lower than the expected value, 90:10 instead of 75:25. On the basis of the true composition this electrocatalysts will be denoted as Pt_9Cr/C.

Figure 1a shows the X-ray diffraction patterns of Pt_9Cr/C made by the BM and of commercial Pt/C, Pt_3Cr/C and PtCr/C alloy electrocatalysts. Detailed Pt (220) peaks of the binary electrocatalysts are shown in Figure 1b. As indicated in Figure 1, all the XRD patterns clearly show the five main characteristic peaks of the face-centred cubic (fcc) crystalline Pt, namely, the planes (111), (200), (220), (311), and (222). These five diffraction peaks in the Pt–Cr/C alloy electrocatalysts are slightly shifted to higher angles with respect to the corresponding peaks in Pt/C, indicating a contraction of the lattice and alloy formation. No peak for pure Cr and its oxides was found, but their presence cannot be discounted because they may be present in a very small amount or even in an amorphous form. In addition to the five main characteristic peaks of the Pt fcc structure, four weak peaks were found for the PtCr/C electrocatalyst, which were assigned to the superlattice planes of an ordered Pt–Cr alloy phase.

The lattice parameters of Pt/C and Pt–Cr/C alloy electrocatalysts are reported in Table 1. The lattice parameters for all the Pt–Cr/C alloy electrocatalysts are smaller than those for Pt/C and decrease with the increase of Cr content, reflecting a progressive introduction of Cr into the alloyed state. Figure 2 shows the plot of the lattice parameter of carbon supported Pt–Cr alloys obtained for the catalysts used in the present work, i.e., the catalyst prepared by the BM and the catalysts from E-TEK, and those found in the literature [7, 16, 24] vs. the Cr content in the catalyst. As expected on the basis of Vegard's law a linear relation between the lattice parameter and the Cr amount was found, except for the catalyst with 50 at. % Cr from E-TEK. The value of the lattice parameter of the PtCr/C E-TEK catalyst was higher than the value expected from Vegard's law, which is indicative of a poor degree of alloying. Also, the diffraction peaks of the binary electrocatalysts are sharper than those of pure platinum indicating a larger metal particle size. The metal particle size, obtained by Scherrer' equation, and the surface area (SA) calculated by the relation SA (m g^{-1}) $= 6 \times 10^3/\rho d$, where d is the mean metal particle size in nm and ρ is the

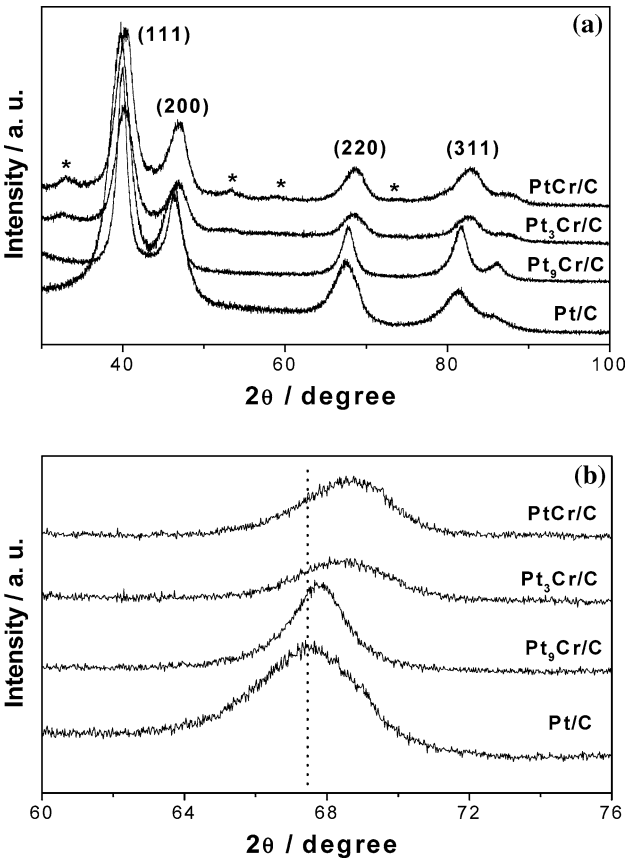

Fig. 1. (a) XRD diffractograms of Pt and Pt–Cr electrocatalysts. (b) Detail of the (220) peaks.

Table 1. EDX composition and structural characteristics by XRD analysis of the carbon supported Pt and Pt–Cr electrocatalysts

Catalyst, nominal composition	EDX composition Pt:Cr	Lattice parameter (nm)	Pt–Pt bond distance (nm)	Particle size (nm)	Metal surface area (m^2 g^{-1})
Pt/C E-TEK	(100)	0.3915	0.2768	2.8	100
Pt–Cr/C BM 3:1	90:10	0.3906	0.2762	4.8	62
Pt–Cr/C E-TEK 3:1	74:26	0.3869	0.2735	3.1	103
Pt–Cr/C E-TEK 1:1	52:48	0.3862	0.2731	3.7	105

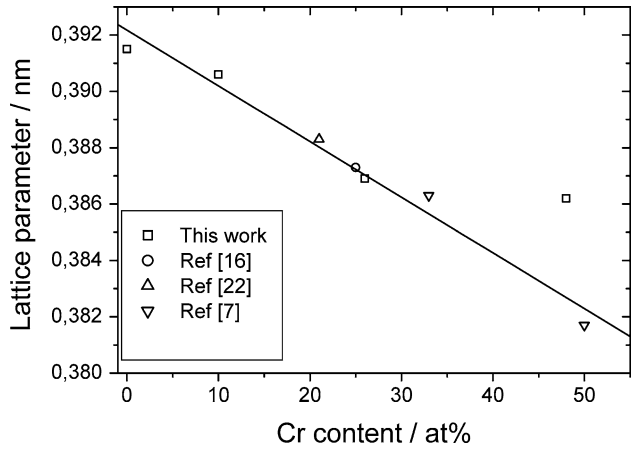

Fig. 2. Dependence of the lattice parameter on the Cr content in the catalyst.

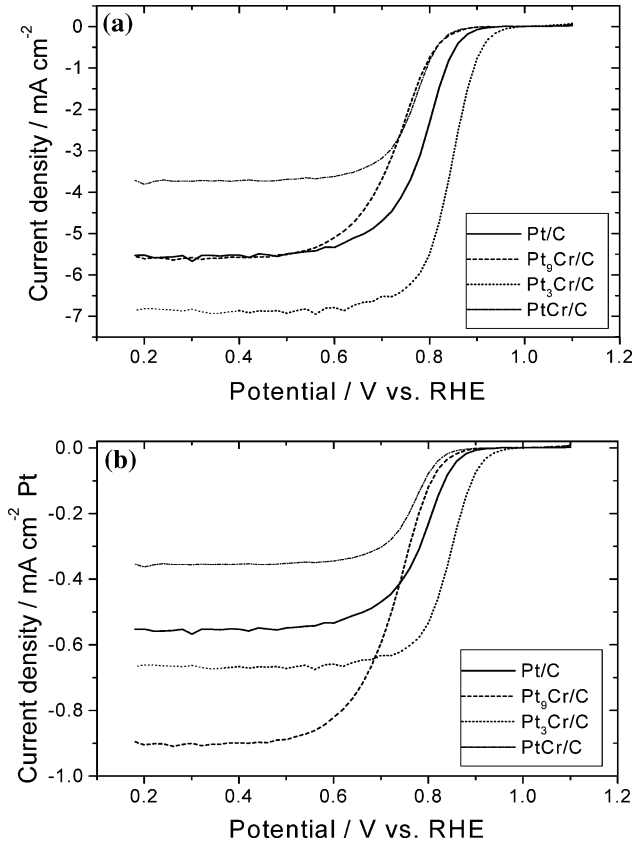

Fig. 3. Steady-state polarization curves for O_2 reduction at 1600 rpm in 1 mol l^{-1} H_2SO_4 at 25 °C for Pt/C and Pt–Cr/C electrocatalysts. (a) Current density normalized with respect to the geometric area; (b) Current density normalized with respect to the Pt surface area.

density of the Pt or the alloy, are also reported in Table 1.

The experimental results regarding the ORR in pure H_2SO_4 are summarized in Figure 3, where the current density normalized both by the geometric area (Figure 3a) and by the Pt surface area (Figure 3b) is plotted against the potential vs. the reversible hydrogen electrode (RHE). The carbon supported Pt_3Cr alloy electrocatalyst shows the highest activity for the ORR. The onset potential for oxygen reduction was shifted to more positive potentials and the overpotential at current densities of 1 mA cm^{-2} (geometric area) and 0.1 mA cm^{-2} (Pt surface area) was ca. 60 mV lower compared to pure Pt. The overpotential of the Pt_9Cr/C and PtCr/C electrocatalysts at the same current densities were ca. 30–40 mV higher than pure Pt. The limiting current density of Pt_3Cr/C was higher than that of Pt/C both in terms of geometric area and in terms of Pt surface area. The low limiting current of PtCr/C is probably due to the presence of a high amount of Cr oxides. The high limiting current per Pt surface area of Pt_9Cr is related to the large particle size of this catalyst. The superior activity of the Pt_3Cr/C alloy electrocatalyst can be ascribed to a good combination of both the Pt–Pt bond distance and the Pt 5 *d*-band vacancy. Indeed, both the Pt–Pt distance and the Pt *d*-band vacancies vs. alloy composition plots follow a volcano type relationship [16].

Further characterization of the catalytic activity of the Pt/C and Pt–Cr/C electrocatalysts was made using mass-transport corrected Tafel plots, normalized per mass of Pt in the catalyst layer, as shown in Figure 4, by plotting E vs. $|j^*j_L/(j_L-j)|$, where j_L is the diffusion limiting current. In agreement with previous investigations on supported Pt-based catalysts [25, 26], two linear Tafel regions are observed for the ORR in all Pt/C electrocatalysts. In these experiments, because of the very thin catalyst layer, an oxygen concentration gradient within the flooded-agglomerate region is not expected. Thus, the change of the Tafel slope is related exclusively to the change in the mechanism/kinetics of the oxygen reduction electrocatalysis on the Pt surface, as already proposed for smooth [27] or non-porous Pt layers [28]. As shown in Figure 4, in the potential region above 0.74 V vs. RHE, the mass transport corrected Tafel slope is very similar for Pt/C and all the Pt–Cr/C electrocatalysts, varying from 52 to 56 mV $decade^{-1}$. In the potential region below 0.74 V vs. RHE, the Tafel slopes are close to 120 mV $decade^{-1}$. Within the fitting error, the Tafel slope did not show any dependence on

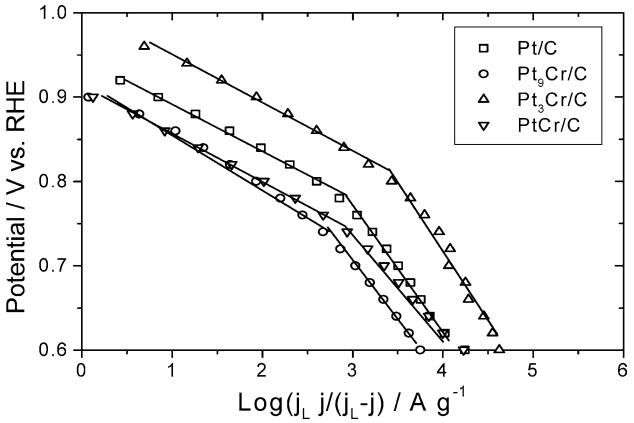

Fig. 4. Tafel plots for the ORR in 1 mol l^{-1} H_2SO_4 (methanol free solution) on Pt/C and Pt–Cr/C catalysts. Current density normalized with respect to the Pt mass.

the composition and structural parameters of the electrocatalysts. Thus, it can be concluded that the addition of chromium to platinum does not involve a change in the reaction mechanism, in agreement with the results of Yang et al. [7] on carbon-supported Pt–Cr alloy electrocatalysts prepared via a Pt-carbonyl route.

The current-potential plots for methanol oxidation in unstirred solutions of 3 mol l^{-1} CH_3OH and 1 mol l^{-1} H_2SO_4 are presented in Figure 5. The methanol-containing electrolyte was previously purged with nitrogen in order to avoid oxygen contamination. It can be seen that the current density for the MOR on Pt_9Cr/C is much lower than that on Pt/C, notwithstanding the larger particle size of this binary catalyst. Indeed, it is known that the activity for methanol oxidation increases with increasing metal particle sizes [29]. Therefore, the current densities increased with increasing Cr content in the alloy, as can be seen in Figure 6, when the current densities normalized for the Pt surface area at 0.7 and 0.8 V are plotted vs. the lattice parameter. The lower MOR activity on Pt_9Cr compared to that of pure Pt can be explained on the basis of the above-mentioned "ensemble effect." Indeed, it is well established that for methanol oxidation at least three adjacent Pt sites in the proper spatial arrangement are necessary to activate the chemisorption of methanol [17–19]. For the PtCr/C alloy electrocatalysts, the probability of finding three neighbouring Pt atoms on the surface is lower if no Pt enrichment of the surface takes place. Since the dissociative chemisorption of methanol requires several adjacent Pt ensembles, the presence of methanol-tolerant Cr around Pt active sites could hinder methanol adsorption on Pt sites due to the dilution effect. On the other hand, oxygen adsorption, which usually can be regarded as dissociative chemisorption and requires only two adjacent Pt sites, is not influenced by the presence of Cr atoms.

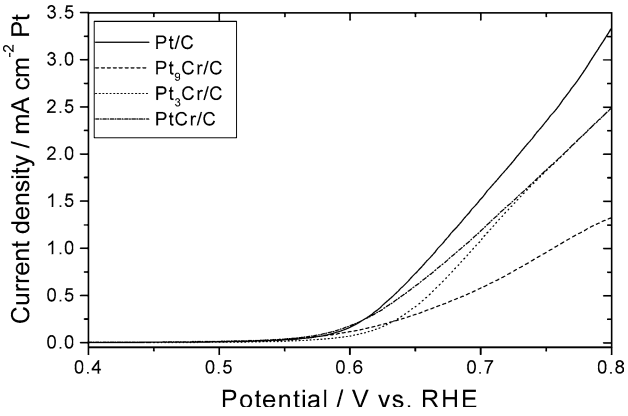

Fig. 5. Anodic scan in 1 mol l^{-1} methanol solution for Pt/C and Pt–Cr/C electrocatalysts. Current density normalized with respect to the Pt surface area.

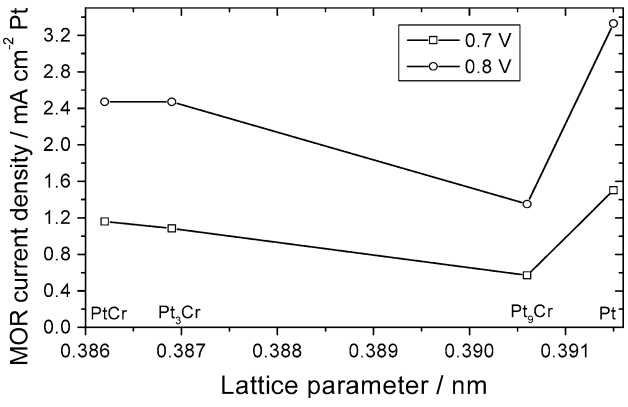

Fig. 6. Dependence of the MOR activity at 0.7 and 0.8 V on the lattice parameter for Pt and Pt–Cr catalysts. Current density normalized with respect to Pt surface area.

However, the presence of Cr atoms reduces the Pt–CO bond strength substantially, enhancing the oxidation of CO. Indeed, it is known that the strong adsorption of OH and CO on small particles (<5 nm) slows the oxidation of methanol, as a result of a significant increase in the *d*-band vacancy at potentials higher than 0.54 V [30]. But such an increase in Pt *d*-band vacancy is reduced by increasing the content of the non-precious metal in the alloy [16]. Then, the electronic effect of alloying explains the increase of the MOR activity with increasing Cr content in the alloy. Thus, 90:10 seems to be an optimum value of the Pt:Cr ratio that maximizes the ensemble effect and minimizes the removal of CO.

The lower MOR activity of the Pt–Cr electrocatalysts compared to that of Pt was confirmed by measurements of the ORR activity in the presence of methanol. Figures 7 and 8 show the ORR activity for the Pt/C and Pt–Cr alloy electrocatalysts in the presence of 1 and 3 mol l^{-1} CH_3OH, respectively, with the current density normalized with respect to both the geometric area (Figures 7a and 8a) and the Pt surface area (Figures 7b and 8b). As compared to the ORR in pure H_2SO_4 solution (cf. Figure 3), all the electrocatalysts showed an increase in overpotential for the ORR under the same current density in the presence of methanol.

The significant increase in the overpotential of the ORR on pure Pt and Pt–Cr alloy electrocatalysts is due to the competitive reaction between oxygen reduction and methanol oxidation. But the overpotential of the ORR on the Pt_9Cr electrocatalyst increases less than in pure Pt and in the other PtCr electrocatalysts, as can be clearly seen in Figure 9, where the potentials at the onset of the ORR and at a current density of 1 mA cm^{-2} (geometric area) are plotted against the lattice parameter of the alloy. Thus, it seems that to attain a good ORR activity the methanol tolerance of the catalyst is more important (in O_2-free methanol solutions Pt_9Cr is the less active electrocatalyst for methanol oxidation) than the intrinsic ORR activity (Pt_3Cr is the electrocatalyst with the highest activity for oxygen reduction). It is interesting to note that the increase of the potential loss (difference between the potential in the absence and the potential in the presence of methanol) in going from 1 to 3 mol l^{-1} CH_3OH concentration is higher for the Pt_9Cr catalyst (ca. 50 mV) than for the others catalysts (ca. 10 mV). When the current density was normalized with respect to

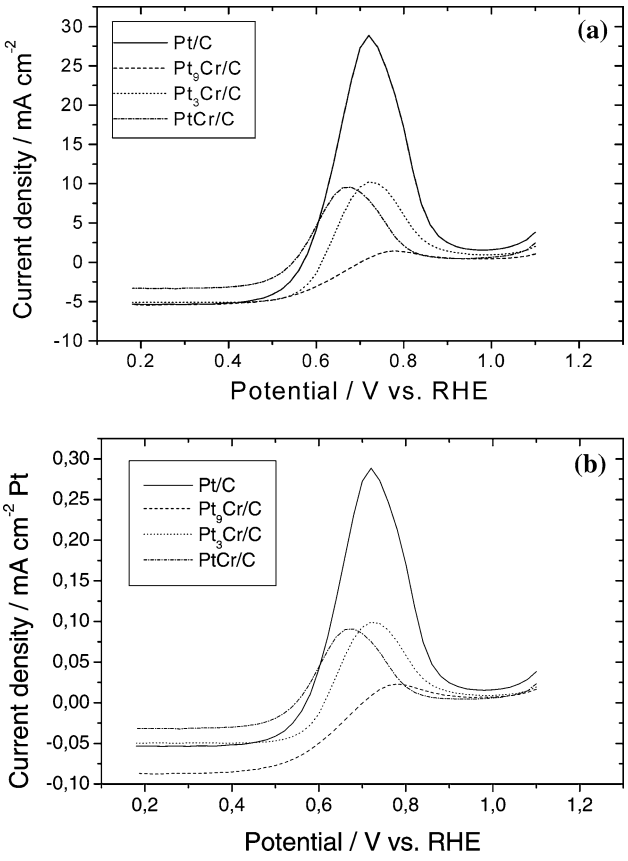

Fig. 7. Steady-state polarization curves for O_2 reduction at 1600 rpm in 0.5 mol l^{-1} H_2SO_4/1 mol l^{-1} CH_3OH at 25 °C for Pt/C and Pt–Cr/C catalysts. (a) Current density normalized with respect to the geometric area; (b) Current density normalized with respect to the Pt surface area.

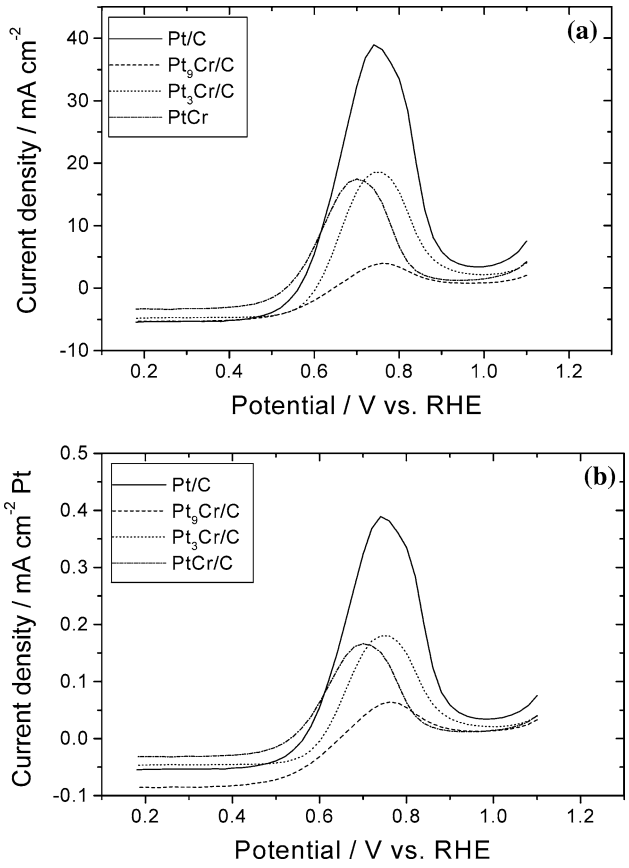

Fig. 8. Steady-state polarization curves for O_2 reduction at 1600 rpm in 0.5 mol l^{-1} H_2SO_4/3 mol l^{-1} CH_3OH at 20 °C for Pt/C and Pt–Cr/C catalysts. (a) Current density normalized with respect to the geometric area; (b) Current density normalized with respect to the Pt surface area.

the Pt surface area the resulting plots were similar to those in which the current density was normalized with respect to the geometric area.

The dependence of the maximum current density for methanol oxidation in oxygen saturated solutions on the lattice parameter for the Pt and Pt alloy electrocatalysts is shown in Figure 10. The dependence of the maximum current density for the MOR on the Cr content in the alloys is in agreement with the results for the MOR activity in oxygen-free methanol.

The DMFC polarization curves for these Pt-based cathode electrocatalysts are shown in Figure 11, with the current density normalized with respect to both the geometric area (Figure 11a) and the Pt surface area (Figure 11b). When the current is expressed in terms of geometric area (mass activity) the cell performances were similar for all the electrocatalysts. In terms of Pt surface area the Pt_9Cr/C electrocatalyst showed the best performance, in agreement with the results for the ORR in the presence of CH_3OH obtained in the rotating disk experiments. The poor performance of PtCr/C as compared with other Pt–M/C catalysts may be due to the presence of significant amounts of oxidized chromium.

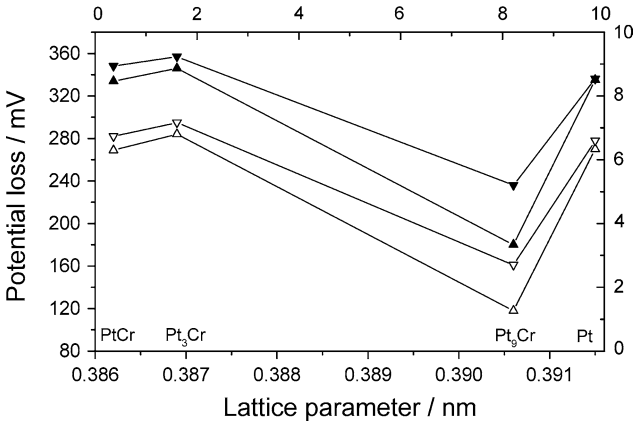

Fig. 9. Dependence of the potential loss on the lattice parameter for Pt and Pt–Cr electrocatalysts. Solid symbols: MOR onset; open symbols: current density of 1 A cm^{-2} (geometric area). Down triangles: 1 mol l^{-1} CH_3OH; up triangles: 3 mol l^{-1} CH_3OH.

4. Conclusions

The experimental findings for the ORR in the absence and presence of methanol on carbon-supported Pt–Cr alloy catalysts can be summarized as follows:

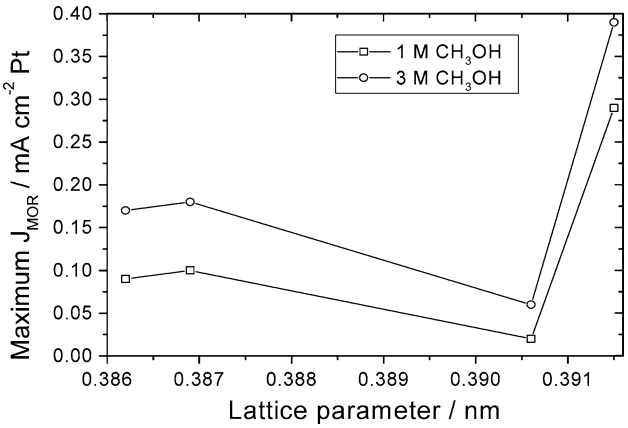

Fig. 10. Dependence of the maximum current density for the MOR in the presence of oxygen on the lattice parameter for Pt and Pt–Cr electrocatalysts.

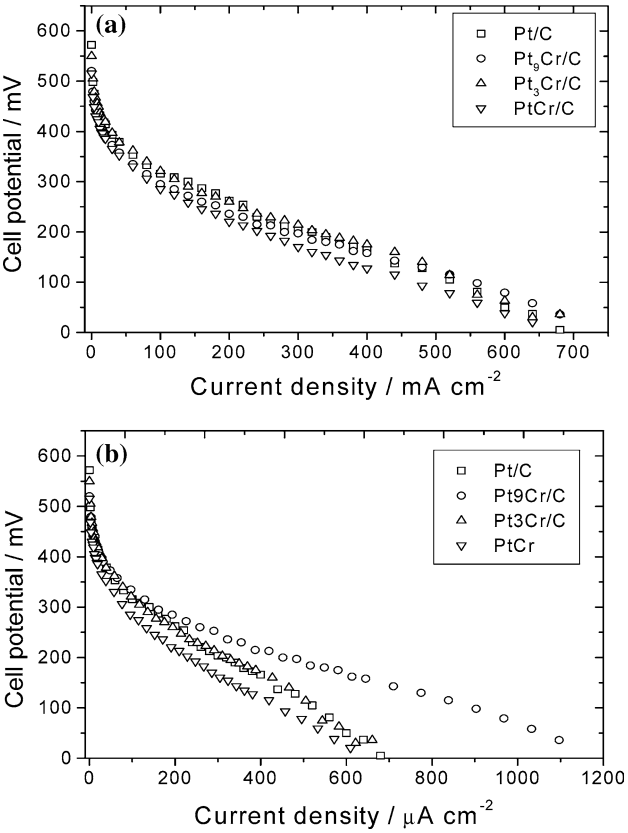

Fig. 11. Polarization curves in single DMFC with Pt/C and Pt–Cr/C as cathode electrocatalysts at 90 °C and 3 atm O_2 pressure using a 2 mol l^{-1} methanol solution. Anode with Pt/C electrocatalyst. (a) Current densities normalized with respect to the geometric area (MA). (b) Current densities normalized with respect to the Pt surface area (SA).

1. In 1 mol l^{-1} H_2SO_4 the Pt_3Cr/C alloy catalyst showed the best activity for the ORR.
2. In O_2-free 1 mol l^{-1} H_2SO_4/3 mol l^{-1} CH_3OH the lowest activity for the MOR was observed with the Pt_9Cr/C catalyst.
3. The best activity for the ORR in 1 mol l^{-1} H_2SO_4/ 1–3 mol l^{-1} CH_3OH was presented by the Pt_9Cr/C electrocatalyst. Thus, it seems that to achieve a good activity for the ORR in the presence of methanol, the methanol tolerance of the catalyst is more important than its intrinsic ORR activity.
4. In DMFC, when the current density was expressed in terms of mass activity, the cell performances were close for all the catalysts. When the current density was normalized with respect to the Pt surface area, instead, the best performance was shown by the cell with Pt_9Cr/C as cathode catalyst.

Acknowledgements

The authors thank the Conselho Nacional de Desenvolvimento Científico e Tecnológico (CNPq, Proc. 140205/2001-2) and the Fundação de Amparo a Pesquisa do Estado de São Paulo (FAPESP, Proc. 99/06430-8 and Proc. 03/04334-9) for financial support. Financial support from Gobierno Autónomo de Canarias (PI2003/070), and GES (MAT2002-01685, Feder) is also gratefully acknowledged. G.G. thanks the MCYT for a FPI Grant (BES-2003-0919).

References

1. X. Ren, P. Zelenay, S. Thomas, J. Davey and S. Gottesfeld, *J. Power Sources* **86** (2000) 111.
2. B. Gurau and E.S. Smotkin, *J. Power Sources* **112** (2002) 3339.
3. P.M. Urban, A. Funke, J.T. Muller, M. Himmen and A. Docter, *Appl. Catal. A* **221** (2001) 459.
4. A. Heinzel and V.M. Barragan, *J. Power Sources* **84** (1999) 70.
5. K. Ramya and K.S. Dhathathreyan, *J. Electroanal. Chem.* **542** (2003) 109.
6. J. Cruickshank and K. Scott, *J. Power Sources* **70** (1998) 40.
7. H. Yang, N. Alonso-Vante, J.-M. Leger and C. Lamy, *J. Phys. Chem. B* **108** (2004) 1938.
8. A.K. Shukla, R.K. Raman, N.A. Choudhury, K.R. Priolkar, P.R. Sarode, S. Emura and R. Kumashiro, *J. Electroanal. Chem.* **563** (2004) 181.
9. W. Li, W. Zhou, H. Li, Z. Zhou, B. Zhou, G. Sun and Q. Xin, *Electrochim. Acta* **49** (2004) 1045.
10. M. Neergat, A.K. Shukla and K.S. Gandhi, *J. Appl. Electrochem.* **31** (2001) 373.
11. J.R.C. Salgado, E. Antolini and E.R. Gonzalez, *Appl. Catal. B* **57** (2005) 283.
12. J.-F. Drillet, A. Ee, J. Friedemann, R. Kotz, B. Schnyder and V.M. Schmidt, *Electrochim. Acta* **47** (2002) 1983.
13. V. Jalan and E.J.J. Taylor, *J. Electrochem. Soc.* **130** (1983) 2299.
14. M.T. Paffett, G.J. Berry and S. Gottesfeld, *J. Electrochem. Soc.* **135** (1988) 1431.
15. T. Toda, H. Igarashi, H. Uchida and M. Watanabe, *J. Electrochem. Soc.* **146** (1999) 3750.
16. S. Mukerjee, S. Srinivasan, M.P. Soriaga and J. McBreen, *J. Electrochem. Soc.* **142** (1995) 1409.
17. N.M. Markovic and P.N. Ross, *Surface Sci. Rep.* **45** (2002) 121.
18. C. Lamy, A. Lima, V. Le Rhun, C. Coutanceau and J.-M. Leger, *J. Power Sources* **105** (2002) 283.
19. H.A. Gasteiger, N.M. Markovic, P.N. Ross and E.J. Cairns, *Electrochim. Acta* **39** (1994) 1825.
20. J.R.C. Salgado and E.R. Gonzalez, *Eclet. Quim.* **28** (2003) 77.
21. J.R.C. Salgado, E. Antolini and E.R. Gonzalez, *J. Electrochem. Soc.* **151** (2004) A2143.

22. B.E. Warren, *X-ray Diffraction* (Addison-Wesley, Reading, MA, 1969).
23. Y.P. Mascarenhas and J.M.V. Pinheiro, *Programa para Calculo de Parametro de Rede pelo Metodo de Minimos Quadrados* (SBPC, 1985).
24. M.K. Min, J. Cho, K. Cho and H. Kim, *Electrochim. Acta* **45** (2000) 4211.
25. J. Perez, E.R. Gonzalez and E.A. Ticianelli, *Electrochim. Acta* **44** (1998) 1329.
26. J. Perez, A.A. Tanaka, E.R. Gonzalez and E.A. Ticianelli, *J. Electrochem. Soc.* **141** (1998) 431.
27. D.B. Sepa, M.V. Vojnovic, L.J.M. Vracar and A. Damjanovic, *Electrochim. Acta* **269** (1981) 781.
28. K. Tammeveski, T. Tenno, J. Claret and C. Ferrater, *Electrochim. Acta* **42** (1997) 893.
29. Y. Takasu, T. Iwazaki, W. Sugimoto and Y. Murakami, *Electrochem. Commun.* **2** (2000) 671.
30. S. Mukerjee and J. McBreen, *J. Electrochem. Soc.* **143** (1996) 2285.